A HIGH ACCURACY NONCONFORMING FINITE ELEMENT SCHEME FOR HELMHOLTZ TRANSMISSION EIGENVALUE PROBLEM

YINGXIA XI, XIA JI, AND SHUO ZHANG

ABSTRACT. In this paper, we consider a cubic H^2 nonconforming finite element scheme B_{h0}^3 which does not correspond to a locally defined finite element with Ciarlet's triple but admit a set of local basis functions. For the first time, we deduce and write out the expression of basis functions explicitly. Distinguished from the most nonconforming finite element methods, $(\delta \Delta_h \cdot, \Delta_h \cdot)$ with non-constant coefficient $\delta > 0$ is coercive on the nonconforming B_{h0}^3 space which makes it robust for numerical discretization. For fourth order eigenvalue problem, the B_{h0}^3 scheme can provide $O(h^2)$ approximation for the eigenspace in energy norm and $O(h^4)$ approximation for the eigenvalues. We test the B_{h0}^3 scheme on the vary-coefficient bi-Laplace source and eigenvalue problem, further, transmission eigenvalue problem. Finally, numerical examples are presented to demonstrate the effectiveness of the proposed scheme.

1. INTRODUCTION

Recently the transmission eigenvalue problem has been attracting interests from many researchers. This problem arose in the inverse scattering theory for inhomogeneous medium and plays a key role in inverse scattering theory. The transmission eigenvalues can be used to obtain estimates for the physical characteristics of the hidden scatterer and have a variety of applications in inverse problem, such as target identification and nondestructive testing [4] [9]. Besides, transmission eigenvalues can also be used to design the invisible material [12].

Typically, for the scattering of time-harmonic acoustic waves by a bounded simply connected inhomogeneous medium $\Omega \subset \mathcal{R}^2$, the transmission eigenvalue problem is to find $k \in C$, $\phi, \varphi \in$

$H^2(\Omega)$ such that

$$
\begin{cases}
\Delta\phi + k^2 n(x)\phi &= 0, \quad \text{in } \Omega, \\
\Delta\varphi + k^2\varphi &= 0, \quad \text{in } \Omega, \\
\phi - \varphi &= 0, \quad \text{on } \partial\Omega, \\
\frac{\partial\phi}{\partial\nu} - \frac{\partial\varphi}{\partial\nu} &= 0, \quad \text{on } \partial\Omega,
\end{cases}
$$

where $n(x)$ is the index of refraction and ν is the unit outward normal to the boundary $\partial\Omega$. Typically, it's assumed that $n(x) > 1$ or $0 < n(x) < 1$.

The transmission eigenvalue problem is non-self-adjoint and not covered by the standard theory of partial differential equations. It is numerically challenging because of the nonlinearity and the complicated spectral. Moreover, in most cases, the continuous problem degenerates with an infinite dimensional eigenspace associated with the zero eigenvalue, which has no physical meaning and makes it difficult to be solved. The first numerical study may be found in [7] where three finite element methods were proposed. In [18], the author reformulates the transmission eigenvalue problem as the combination of a nonlinear function and a series of fourth order self-adjoint eigenvalue problems. The roots of the nonlinear function are the transmission eigenvalues., and an iterative method was proposed based on this. The rigorous convergence analysis was first given. But this method can only capture real eigenvalues.

To avoid the non-physical eigenspaces, introducing a new variable $u = \phi - \varphi \in H_0^2(\Omega)$, following the same procedure in [13], we can obtain the following fourth order equation

$$
(1) \qquad (\Delta + k^2 n(x))\frac{1}{n(x) - 1}(\Delta + k^2)u = 0.
$$

We remark that the above fourth order equation has eliminated the non-physical zero eigenvalue. Actually $k = 0$ implies $(\frac{1}{n(x) - 1}\Delta u, \Delta u) = 0$ and $u \in H_0^2(\Omega)$, and then we can obtain $u = 0$. The corresponding variational formulation of (1) is to find $(k^2 \neq 0, u) \in \mathbb{C} \times H_0^2(\Omega)$, such that

$$
(2) \qquad \left(\frac{1}{n(x) - 1}(\Delta u + k^2 u), \Delta v + k^2 n(x)v\right) = 0, \quad \forall\, v \in H_0^2(\Omega).
$$

Let $\tau = k^2$ (we also call τ a transmission eigenvalue if k is), the corresponding variational form is to find $(\tau \neq 0, u) \in \mathbb{C} \times H_0^2(\Omega)$, such that

$$
(3) \qquad \left(\frac{1}{n(x) - 1}(\Delta u + \tau u), \Delta v + \tau n(x)v\right) = 0, \quad \forall\, v \in H_0^2(\Omega).
$$

Here we consider the case $n(x) > 1$ for illustration. For the case $0 < n(x) < 1$, it follows similarly. Using Green formula, we can rewrite the original variational formulation (3) as

$$
(4) \qquad \mathcal{A}_\tau(u, v) = \tau\mathcal{B}(u, v), \quad \forall v \in V,
$$

where

$$(5) \qquad \mathcal{A}_\tau(u, v) \;=\; \Big(\frac{1}{n(x) - 1} (\Delta u + \tau u), (\Delta v + \tau v) \Big) + \tau^2 (u, v),$$

and

$$(6) \qquad \mathcal{B}(u, v) \;=\; (\nabla u, \nabla v).$$

The bilinear form $\mathcal{A}_\tau(\cdot, \cdot)$ is coercive on $H_0^2(\Omega) \times H_0^2(\Omega)$, and the bilinear form $\mathcal{B}(\cdot, \cdot)$ is symmetric and nonnegative on $H_0^2(\Omega) \times H_0^2(\Omega)$ [3, 18].

The finite element discretization of (1) is natural. Many schemes, such as the Argyris element method [7], the (multi-level) BFS element method [14], the Morley element method [16,20], the modified Zienkiewciz element and the Morley-Zienkiewicz element [23] and other low complexity finite element methods including an interior penalty discontinuous Galerkin method using C^0 Lagrange elements (C^0IPG method) [8], and so on. There have also existed some mixed methods for this problem. The related works for mixed element method can be referred to [5, 7, 13, 21, 22]. The mixed scheme in [5, 13] which is close to the Ciarlet-Raviart discretization of biharmonic problem is based on Lagrange finite element method. For the nonzero transmission eigenvalues, this scheme is equivalent to the one proposed in [7]. However, the scheme in [5, 13] can eliminate the zero transmission eigenvalue which has an infinite dimensional space and has no physical meaning. A mixed formulation in terms of three scaler fields and a spectral-mixed method are constructed in [22]. In [21], the authors propose a multi-level mixed formulation in terms of seven scaler fields. An equivalent linear mixed formulation of transmission eigenvalue problem which doesn't produce spurious modes even on non-convex domains is constructed. The proposed scheme admits a natural nested discretization, based on that a multi-level scheme is built. Optimal convergence rate and optimal computational cost can be obtained.

The finite element discretization of (4) looks immediate. While a $(\Delta \cdot, \Delta \cdot)$ bilinear form is used in the formulation, however, we have to note that $(\Delta_h \cdot, \Delta_h \cdot)$ is not coercive on general nonconforming finite element spaces. A standard approach is to enhance the bilinear from with $\alpha(\nabla^2 \cdot, \nabla^2 \cdot)$ for stabilisation, where α is a parameter. It is then not surprising that the choice of α may effect the performance of the scheme; a detailed illustration of the sensitivity of α can be found in Sections 2.4 and 3.2. To strengthen the robustness of the scheme, a finite element space which is of low degree and on which the bilinear form $(\Delta_h \cdot, \Delta_h \cdot)$ is coercive is needed.

In this paper, we introduce a new scheme for the Helmholtz transmission eigenvalue problem. Basically, we adapt onto (4) a piecewise cubic finite element space B_{h0}^3 introduced in [24,25]. It is proved that B_{h0}^3 provide $O(h^2)$ accuracy on both approximation error in broken H^2 error and

consistency error associated to the biharmonic operator. Moreover, it is proved in [25] that

$$(\Delta_h u_h, \Delta_h v_h) = (\nabla_h^2 u_h, \nabla_h^2 v_h), \ \forall \, u_h, v_h \in B_{h0}^3.$$

Thus a finite element scheme based on B_{h0}^3 for the transmission eigenvalue problem can provide $O(h^2)$ approximation for the eigenspace in energy norm and $O(h^4)$ approximation for the eigenvalues. Numerical experiments of this paper verify this.

The space B_{h0}^3 does not correspond to a finite element defined by Ciarlet's triple, however, it admits a set of local basis functions [24]. By following the procedure given in [24,25], the finite element scheme designed in this paper can be implemented without knowing the basis functions of B_{h0}^3. However, in the order that basic algorithms can be used, the local basis functions are still in need, and we figure out them in this paper.

The rest of this paper is organized as follows. In Section 2, we study the finite element space B_{h0}^3 and its utilization for the bi-Laplacian operator. We particularly figure out its local basis functions and illustrate the performance of the scheme with numerical examples. An illustration about the Morley element onto the model problem is also given for comparison. Section 3 is devoted to the Helmholtz transmission eigenvalue problem. Numerical experiments are given, including those of the Morley element for comparison. Finally, some concluding remarks are given in Section 4.

2. A high-accuracy scheme for bi-Laplacian problem with varying coefficient

In this section, we first consider the following fourth order eigenvalue problem

$$(7) \qquad \begin{cases} \Delta(\delta\Delta u) &=& \lambda u, & \text{in } \Omega, \\ u &=& 0, & \text{on } \partial\Omega, \\ \frac{\partial u}{\partial n} &=& 0, & \text{on } \partial\Omega, \end{cases}$$

where $\delta(x)$ is a bounded smooth non-constant function and $\delta \geqslant \delta_{\min} > 0$.

2.1. **A piecewise cubic finite element space and its structure.** Before introducing this finite element, we introduce some notations. We assume $\mathcal{T}_h$ a shape regular mesh over Ω with mesh size h. Denote $\mathcal{X}_h$, $\mathcal{X}_h^i$, $\mathcal{X}_h^b$, $\mathcal{E}_h$, $\mathcal{E}_h^i$, $\mathcal{E}_h^b$ the vertices, interior vertices, boundary vertices, the set of edges, interior edges and boundary edges, respectively. For any edge $e \in \mathcal{E}_h$, denote the unit normal vector of e by $\mathbf{n_e}$. For a fixed element $T \in \mathcal{T}_h$, we denote $\mathcal{P}_k(T)$ the polynomial space of degree less than or equal to k and $|T|$ means the area measurement of element T. On an edge e, $\mathcal{P}_k(e)$ and $|e|$ are defined similarly. The barycentre coordinates are denoted as usual by $\lambda_i (i = 1, 2, 3)$.

The nonconforming finite element space B_h^3 can be defined as follows: ([24, 25])

$$B_h^3 = \{v \in L^2(\Omega) \mid v|_T \in \mathcal{P}_3(T), \ v \text{ is continuous at vertices } a \in \mathcal{X}_h \text{ and}$$

$$\int_e [\![v]\!] \, ds = 0, \text{ and } \int_e p_e [\![\partial_n v]\!] \, ds = 0, \ \forall \ p_e \in P_1(e), \ \forall \ e \in \mathcal{E}_h^i, \ \forall \ T \in \mathcal{T}_h\}$$

where $[\![v]\!]$ represents the jump of the scalar function v across e, and

$$B_{h0}^3 = \{v \in B_h^3 \mid v(a) = 0, a \in \mathcal{X}_h^b; \int_e v \, ds = 0, \text{ and } \int_e p_e \partial_n v \, ds = 0, \ \forall \ p_e \in P_1(e), \ \forall \ e \in \mathcal{E}_h^b\}.$$

Lemma 1. *[24, 25]* $\inf_{w_h \in B_{h0}^3} |w - w_h|_{2,h} \leqslant Ch^k |w|_{2+k,\Omega}, \ \forall \ w \in H_0^2(\Omega) \cap H^{k+2}(\Omega), \ \ k = 1, 2.$

Local basis functions of B_{h0}^3. The space B_{h0}^3 does not correspond to a locally defined finite element with Ciarlet's triple. However, it is pointed out that the space admits a set of local basis functions. In the following, we will deduce and write out the expressions of basis functions in detail. The derivation is based on the thought raised in [24] and we need the following results.

Lemma 2. *([24]) B_{h0}^3 admits a set of basis functions with vertex-patch-based supports.*

The following lemma involves the vector-valued finite element spaces $\widetilde{S}_{h0}^2(rot, w_0), \widetilde{G}_{h0}^2(rot_h, 0)$ of which the definition concerns a series of definitions of associated finite element spaces. It's omitted here and the author can refer the detail to [24]. And we use "~" for vector valued quantities in the following. And $\widetilde{\varphi}^1, \widetilde{\varphi}^2$ are the two components of the quantity $\widetilde{\varphi}$.

Lemma 3. *([24]) Define an operator $\mathcal{F}_h : \widetilde{S}_{h0}^2(rot, w_0) \longrightarrow \widetilde{G}_{h0}^2(rot_h, 0)$ by*

$$\mathcal{F}_h \widetilde{\varphi}_h = \widetilde{\varphi}_h + \widetilde{\phi}_h, \ \ \forall \widetilde{\varphi}_h \in \widetilde{S}_{h0}^2(rot, w_0), \ \ \widetilde{\phi}_h \in \widetilde{B}_{h0}^2, \ s.t. \ rot_h(\mathcal{F}_h \widetilde{\varphi}_h) = 0,$$

where $\widetilde{B}_{h0}^2 = \{\widetilde{\phi}_h : \ (\widetilde{\phi}_h|_T)^j \in \ span\{(\lambda_1^2 + \lambda_2^2 + \lambda_3^2) - 2/3\}, \ j = 1, 2, \ \forall \ T \in \mathcal{T}_h\}$. And define $(\nabla^{-1})_h : \widetilde{G}_{h0}^2(rot_h, 0) \longrightarrow B_{h0}^3$, then $(\nabla^{-1})_h \circ \mathcal{F}_h : \widetilde{S}_{h0}^2(rot, w_0) \longrightarrow B_{h0}^3$ is bijective and preserves support.

From Lemma 3, it can be observed that there are three steps in the derivations of basis functions. We orderly construct the basis functions in $\widetilde{S}_{h0}^2(rot, w_0), \widetilde{G}_{h0}^2(rot_h, 0)$ and B_{h0}^3. Before introducing the derivation, we give some definitions. For $a \in \mathcal{X}_h$, denote by P_a the union of triangles of which a is a vertex, namely the patch associated with a; for $e \in \mathcal{E}_h$, denote by P_e the patch associated with e.

First, we consider constructing the basis functions in $\widetilde{S}_{h0}^2(rot, w_0)$ with vertex-patch-based supports. On every vertex (e.g: denoted by a), three basis functions are associated, which are labelled as $\widetilde{\varphi}_a^x, \widetilde{\varphi}_a^y, \widetilde{\varphi}_{P_a}$. And on every edge (e.g: denoted by e), one basis function is

associated, which is labelled as $\widetilde{\varphi}_e$. For every basis function associated with an interior vertex a, its restriction on a cell T such that a is a node of T. For every basis function associated with an edge, its restriction on a cell T such that e is an edge of T. Then we can only focus on an element and give out the basis functions.

For the construction of $\widetilde{\varphi}_a^x$, $\widetilde{\varphi}_a^y$, $\widetilde{\varphi}_{P_a}$ and $\widetilde{\varphi}_e$, we follow the thought in [24] and have the guaranteed theoretical result.

Lemma 4. *([24]) The set $\{\widetilde{\varphi}_a^x, \widetilde{\varphi}_a^y, \widetilde{\varphi}_{P_a}, \widetilde{\varphi}_e\}_{a\in\mathcal{X}_h^i,\ e\in\mathcal{E}_h^i}$ forms a basis of $\widetilde{S}_{h0}^2(rot, w_0)$.*

For a fixed element $T \in \mathcal{T}_h$, the vertex denoted by $i(i = 1, 2, 3)$, the opposite side of vertex i denoted by e_i. For the vertex i and its opposite edge e_i, the associated basis functions are as follows.

- $\widetilde{\varphi}_i^x = ((\widetilde{\varphi}_i^x)^1, (\widetilde{\varphi}_i^x)^2)^T = (\lambda_i - 3\lambda_i\lambda_j - 3\lambda_i\lambda_k, 0)^T = (3\lambda_j^2 + 6\lambda_j\lambda_k + 3\lambda_k^2 - 4\lambda_j - 4\lambda_k + 1, 0)^T,$

- $\widetilde{\varphi}_i^y = ((\widetilde{\varphi}_i^y)^1, (\widetilde{\varphi}_i^y)^2)^T = (0, \lambda_i - 3\lambda_i\lambda_j - 3\lambda_i\lambda_k)^T = (0, 3\lambda_j^2 + 6\lambda_j\lambda_k + 3\lambda_k^2 - 4\lambda_j - 4\lambda_k + 1)^T,$

- $\widetilde{\varphi}_e^i = ((\widetilde{\varphi}_e^i)^1, (\widetilde{\varphi}_e^i)^2)^T = \dfrac{6\lambda_j\lambda_k}{|e_i|}(-\tau_2(e_i), \tau_1(e_i))^T,$

- $\widetilde{\varphi}_{P_i} = ((\widetilde{\varphi}_{P_i})^1, (\widetilde{\varphi}_{P_i})^2)^T = \dfrac{6\lambda_i\lambda_j}{|e_k|}(\tau_1(e_k), \tau_2(e_k))^T + \dfrac{6\lambda_i\lambda_k}{|e_j|}(\tau_1(e_j), \tau_2(e_j))^T$

$$= \dfrac{6(1 - \lambda_j - \lambda_k)\lambda_j}{|e_k|}(\tau_1(e_k), \tau_2(e_k))^T + \dfrac{6(1 - \lambda_j - \lambda_k)\lambda_k}{|e_j|}(\tau_1(e_j), \tau_2(e_j))^T,$$

where i, j, k satisfy the cyclic coordinate.

Second, we consider constructing the basis functions in $\widetilde{G}_{h0}^2(rot_h, 0)$. By Lemma 3 and its process of proof in [24], it's easy to verify the following conclusion.

Lemma 5. *Under the assumption that $\{\widetilde{\varphi}_a^x, \widetilde{\varphi}_a^y, \widetilde{\varphi}_{P_a}, \widetilde{\varphi}_e\}_{a\in\mathcal{X}_h^i,\ e\in\mathcal{E}_h^i}$ forms a basis of $\widetilde{S}_{h0}^2(rot, w_0)$,*

then $\{\mathcal{F}_h\widetilde{\varphi}_a^x, \mathcal{F}_h\widetilde{\varphi}_a^y, \mathcal{F}_h\widetilde{\varphi}_{P_a}, \mathcal{F}_h\widetilde{\varphi}_e\}_{a\in\mathcal{X}_h^i,\ e\in\mathcal{E}_h^i}$ forms a basis of $\widetilde{G}_{h0}^2(rot, 0)$ and

$supp(\mathcal{F}_h\widetilde{\varphi}_a^x) \subset supp(\widetilde{\varphi}_a^x),\ supp(\mathcal{F}_h\widetilde{\varphi}_a^y) \subset supp(\widetilde{\varphi}_a^y),\ supp(\mathcal{F}_h\widetilde{\varphi}_{P_a}) \subset supp(\widetilde{\varphi}_{P_a}),\ supp(\mathcal{F}_h\widetilde{\varphi}_e) \subset supp(\widetilde{\varphi}_e).$

The above lemma tells us that $\mathcal{F}_h$ can preserve the linear independence and the support of basis functions. Then, for an element $T \in \mathcal{T}_h$, $\mathcal{F}_h\widetilde{\varphi}_i^x$, $\mathcal{F}_h\widetilde{\varphi}_i^y$, $\mathcal{F}_h\widetilde{\varphi}_{P_i}$, $\mathcal{F}_h\widetilde{\varphi}_{e_i}(i = 1, 2, 3)$ are the corresponding basis functions in $\widetilde{G}_{h0}^2(rot_h, 0)$.

Denote $\phi_T = \lambda_1^2 + \lambda_2^2 + \lambda_3^2 - 2/3$ and $\widehat{\varphi}_i^x \triangleq \mathcal{F}_h\widetilde{\varphi}_i^x \in \widetilde{G}_{h0}^2(rot_h, 0)$. By Lemma 3, we assume

$$\widehat{\varphi}_i^x = \widetilde{\varphi}_i^x + (\alpha_i^x, \beta_i^x)^T\phi_T, \quad rot_h\widehat{\varphi}_i^x = 0.$$

By calculation, we can obtain

$$\alpha_i^x = \frac{[(\lambda_k)_x - (\lambda_j)_x][(\lambda_k)_y + (\lambda_j)_y]}{(\lambda_k)_y(\lambda_j)_x - (\lambda_k)_x(\lambda_j)_y}, \quad \beta_i^x = \frac{[(\lambda_k)_y - (\lambda_j)_y][(\lambda_k)_y + (\lambda_j)_y]}{(\lambda_k)_y(\lambda_j)_x - (\lambda_k)_x(\lambda_j)_y}.$$

Similarly, for $\mathcal{F}_h\widetilde{\varphi}_i^y = \widetilde{\varphi}_i^y + (\alpha_i^y, \beta_i^y)^T \phi_T, \mathcal{F}_h\widetilde{\varphi}_e^i = \widetilde{\varphi}_e^i + (\alpha_e^i, \beta_e^i)^T \phi_T, \mathcal{F}_h\widetilde{\varphi}_{P_i} = \widetilde{\varphi}_{P_i} + (\alpha_{P_i}, \beta_{P_i})^T \phi_T$, we have

$$\alpha_i^y = \frac{[(\lambda_j)_x - (\lambda_k)_x][(\lambda_j)_x + (\lambda_k)_x]}{(\lambda_k)_y(\lambda_j)_x - (\lambda_k)_x(\lambda_j)_y}, \quad \beta_i^y = \frac{[(\lambda_j)_y - (\lambda_k)_y][(\lambda_j)_x + (\lambda_k)_x]}{(\lambda_k)_y(\lambda_j)_x - (\lambda_k)_x(\lambda_j)_y}.$$

$$\alpha_e^i = (\lambda_i)_x \frac{6|T|}{|e_i|^2}, \quad \beta_e^i = (\lambda_i)_y \frac{6|T|}{|e_i|^2}.$$

$$\alpha_{P_i} = \frac{-12|T|\nabla\lambda_j\nabla\lambda_k\left\{(\frac{(\lambda_k)_x}{|e_k|^2} + \frac{(\lambda_j)_x}{|e_j|^2})\right\} - \frac{3}{|T|}\left\{(\lambda_j)_x + (\lambda_k)_x\right\}}{2(\lambda_k)_y(\lambda_j)_x - 2(\lambda_k)_x(\lambda_j)_y},$$

$$\beta_{P_i} = \frac{-12|T|\nabla\lambda_j\nabla\lambda_k\left\{(\frac{(\lambda_k)_y}{|e_k|^2} + \frac{(\lambda_j)_y}{|e_j|^2})\right\} - \frac{3}{|T|}\left\{(\lambda_j)_y + (\lambda_k)_y\right\}}{2(\lambda_k)_y(\lambda_j)_x - 2(\lambda_k)_x(\lambda_j)_y}.$$

Here, we consider constructing the basis functions in B_{h0}^3. By Lemma 3 and its process of proof in [24], it's easy to verify the following conclusion.

Lemma 6. *Under the assumption that $\{\widetilde{\varphi}_a^x, \widetilde{\varphi}_a^y, \widetilde{\varphi}_{P_a}, \widetilde{\varphi}_e\}_{a\in X_h^i, e\in \mathcal{E}_h^i}$ forms a basis of $\widetilde{S}_{h0}^2(rot, w_0)$, then $\{(\nabla^{-1})_h \circ \mathcal{F}_h\widetilde{\varphi}_a^x, (\nabla^{-1})_h \circ \mathcal{F}_h\widetilde{\varphi}_a^y, (\nabla^{-1})_h \circ \mathcal{F}_h\widetilde{\varphi}_{P_a}, (\nabla^{-1})_h \circ \mathcal{F}_h\widetilde{\varphi}_e\}_{a\in X_h^i, e\in \mathcal{E}_h^i}$ forms a basis of B_{h0}^3 and*

$$supp\left((\nabla^{-1})_h \circ \mathcal{F}_h\widetilde{\varphi}_a^x\right) \subset supp(\widetilde{\varphi}_a^x), \quad supp\left((\nabla^{-1})_h \circ \mathcal{F}_h\widetilde{\varphi}_a^y\right) \subset supp(\widetilde{\varphi}_a^y),$$

$$supp\left((\nabla^{-1})_h \circ \mathcal{F}_h\widetilde{\varphi}_{P_a}\right) \subset supp(\widetilde{\varphi}_{P_a}), \quad supp\left((\nabla^{-1})_h \circ \mathcal{F}_h\widetilde{\varphi}_e\right) \subset supp(\widetilde{\varphi}_e).$$

Denote $w_i^x = (\nabla^{-1})_h \circ \mathcal{F}_h\widetilde{\varphi}_i^x, w_i^y = (\nabla^{-1})_h \circ \mathcal{F}_h\widetilde{\varphi}_i^y, w_e^i = (\nabla^{-1})_h \circ \mathcal{F}_h\widetilde{\varphi}_e^i, w_{P_i} = (\nabla^{-1})_h \circ \mathcal{F}_h\widetilde{\varphi}_{P_i}$. By calculation, the corresponding basis functions in B_{h0}^3 are as follows.

$$w_i^x(\lambda_j, \lambda_k) = -\xi_k\left\{(\frac{\lambda_j^3}{3} - \lambda_j^2 + \frac{2}{3}\lambda_j) + (\frac{2}{3}\lambda_k^3 - \lambda_k^2 + \frac{\lambda_k}{3}) + (2\lambda_j^2\lambda_k + \lambda_j\lambda_k^2 - 2\lambda_j\lambda_k)\right\} +$$

$$\xi_j\left\{(\frac{2}{3}\lambda_j^3 - \lambda_j^2 + \frac{\lambda_j}{3}) + (\frac{\lambda_k^3}{3} - \lambda_k^2 + \frac{2}{3}\lambda_k) + (2\lambda_j\lambda_k^2 + \lambda_j^2\lambda_k - 2\lambda_j\lambda_k)\right\},$$

$$w_i^y(\lambda_j, \lambda_k) = -\eta_k \left\{ (\frac{\lambda_j^3}{3} - \lambda_j^2 + \frac{2}{3}\lambda_j) + (\frac{2}{3}\lambda_k^3 - \lambda_k^2 + \frac{\lambda_k}{3}) + (2\lambda_j^2\lambda_k + \lambda_j\lambda_k^2 - 2\lambda_j\lambda_k) \right\} +$$

$$\eta_j \left\{ (\frac{2}{3}\lambda_j^3 - \lambda_j^2 + \frac{\lambda_j}{3}) + (\frac{\lambda_k^3}{3} - \lambda_k^2 + \frac{2}{3}\lambda_k) + (2\lambda_j\lambda_k^2 + \lambda_j^2\lambda_k - 2\lambda_j\lambda_k) \right\},$$

$$w_e^i(\lambda_j, \lambda_k) = -\frac{6|T|}{|e_i|^2} \left\{ (\frac{2}{3}\lambda_j^3 - \lambda_j^2 + \frac{\lambda_j}{3}) + (\frac{2}{3}\lambda_k^3 - \lambda_k^2 + \frac{\lambda_k}{3}) + (2\lambda_j^2\lambda_k + 2\lambda_j\lambda_k^2 - 2\lambda_j\lambda_k) \right\},$$

$$w_{P_i}(\lambda_j, \lambda_k) = -3(\eta_j\eta_k + \xi_j\xi_k) \left\{ \frac{1}{|e_j|^2}(\frac{2}{3}\lambda_j^3 - \lambda_j^2 + \frac{\lambda_j}{3}) + \frac{1}{|e_k|^2}(\frac{2}{3}\lambda_k^3 - \lambda_k^2 + \frac{\lambda_k}{3}) + \right\}$$

$$+ 6 \left\{ (-\frac{2}{3}\lambda_j^3 + \lambda_j^2 - \frac{\lambda_j}{6}) + (-\frac{2}{3}\lambda_k^3 + \lambda_k^2 - \frac{\lambda_k}{6}) + (\lambda_j\lambda_k - \lambda_j^2\lambda_k - \lambda_j\lambda_k^2) \right\} - 1,$$

where $i = 1, 2, 3$ which correspond to three vertices of a triangular element and $\xi_i = x_j - x_k$, $\eta_i = y_j - y_k$, i, j, k satisfy the cyclic coordinate.

2.2. A second order computational scheme for bi-Laplacian source and eigenvalue problems.
The bi-Laplacian source problem is to find u satisfying

$$(8) \qquad \begin{cases} \Delta(\delta\Delta u) & = & f, & \text{in } \Omega, \\ u & = & 0, & \text{on } \partial\Omega, \\ \frac{\partial u}{\partial n} & = & 0, & \text{on } \partial\Omega. \end{cases}$$

A finite element scheme for (8) is defined as: find $u_h \in B_{h0}^3$, such that

$$(9) \qquad (\delta\Delta_h u_h, \Delta_h v_h) = (f, v_h), \quad \forall v_h \in B_{h0}^3.$$

Theorem 7. *Let $u \in H^4(\Omega) \cap H_0^2(\Omega)$ be the solution of (8), and u_h be the solution of (9), respectively. Then*

$$|u - u_h|_{2,h} \leqslant Ch^k|u|_{2+k,\Omega}, \quad k = 1, 2,$$

and

$$|u - u_h|_{1,h} \leqslant Ch^3|u|_{4,\Omega}, \quad \text{when } \Omega \text{ is convex.}$$

The finite element space B_{h0}^3 leads immediately to a high-accuracy scheme for the eigenvalue problem of bi-Laplacian equation.

2.3. Numerical experiments.

2.3.1. *For source problems.* **Example 1.** Consider the bi-Laplacian source problem (8) with constant coefficient $\delta = 1$ on square domain $\Omega_1 = [0, 1]^2$ with

$$f = -4\pi^4 \left(\cos(2\pi x) + \cos(2\pi y) - 4 \cos(2\pi x) \cos(2\pi y) \right).$$

The exact solution is $u(x, y) = \sin(\pi x)^2 \sin(\pi y)^2$.

Example 2. Consider the bi-Laplacian source problem (8) with constant coefficient $\delta = 1$ on triangle domain Ω_2 whose vertices are given by $(0, 0), (1, 0), (0, 1)$. And we consider $f = 72(x + y)^2 - 48(x + y) + 8$ for which the exact solution is $u(x, y) = x^2 y^2 (1 - x - y)^2$.

Here we test on **Example 1** and **Example 2**, respectively. The mesh size of the initial mesh is $h_0 = \frac{1}{2}$. Six levels of uniformly refined triangular meshes are generated for numerical experiments and $h_k = h_{k-1}/2, \ k = 1, 2, 3, 4, 5, 6$. The finest degrees of freedom (short for DOFs) for **Example 1** are 97283. The refinest DOFs for **Example 2** are 48387. We discretize by the second order computational scheme corresponding to B_{h0}^3 space. For each series of meshes, we obtain the numerical solution u_{h_k}. The convergent orders measured by $h_2, \ h_1, \ L_2$ norms respectively are computed by

$$log_2 \left(\frac{\|u - u_{h_k}\|_{h_2}}{\|u - u_{h_{k-1}}\|_{h_2}} \right), \quad k = 2, 3, 4, 5, 6,$$

$$log_2 \left(\frac{\|u - u_{h_k}\|_{h_1}}{\|u - u_{h_{k-1}}\|_{h_1}} \right), \quad k = 2, 3, 4, 5, 6,$$

and

$$log_2 \left(\frac{\|u - u_{h_k}\|_{L_2}}{\|u - u_{h_{k-1}}\|_{L_2}} \right), \quad k = 2, 3, 4, 5, 6.$$

For **Example 1**, the errors for numerical solutions are showed in Figure 1(a). For **Example 2**, the errors for numerical solutions are showed in Figure 1(b). We can observe that

(1) The convergence rate for source problem measured by h_2 norm is 2;

(2) The convergence rate for source problem measured by h_1 norm is 3;

(3) The convergence rate for source problem measured by L_2 norm is 4;

which are consistent with the theoretical results.

Example 3. Consider the bi-Laplacian source problem with varying coefficient $\delta = 8 + x_1 - x_2$ on triangle domain Ω_2 whose vertices are given by $(0, 0), (1, 0), (0, 1)$. And we consider $f = 64x^3 + 48x^2 y + 528x^2 - 48xy^2 + 1152xy - 368x - 64y^3 + 624y^2 - 400y + 64$ for which the exact solution is $u(x, y) = x^2 y^2 (1 - x - y)^2$.

For **Example 3**, the errors for numerical solutions are showed in Figure 2. We can observe that

(1) The convergence rate for source problem measured by h_2 norm is 2;
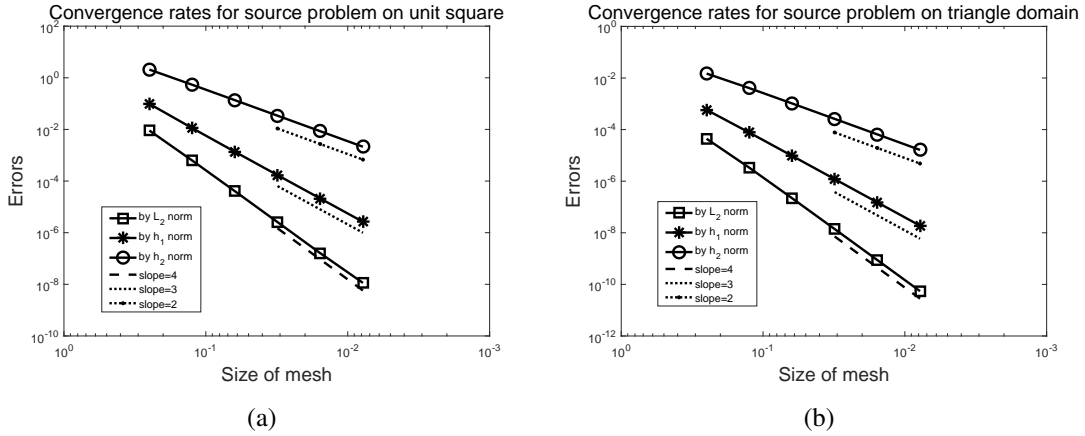
FIGURE 1. The numerical performance for bi-Laplacian source problem by B_{h0}^3. Y-axis means the numerical error $\|u - u_{h_k}\|$ measured by L_2 or h_1 or h_2 norm. X-axis means the size of mesh. Left: for **Example 1** which is on square domain; Right: for **Example 2** which is on triangle domain.

(2) The convergence rate for source problem measured by h_1 norm is 3;

(3) The convergence rate for source problem measured by L_2 norm is 4;

which are optimal and consistent with the theoretical results.
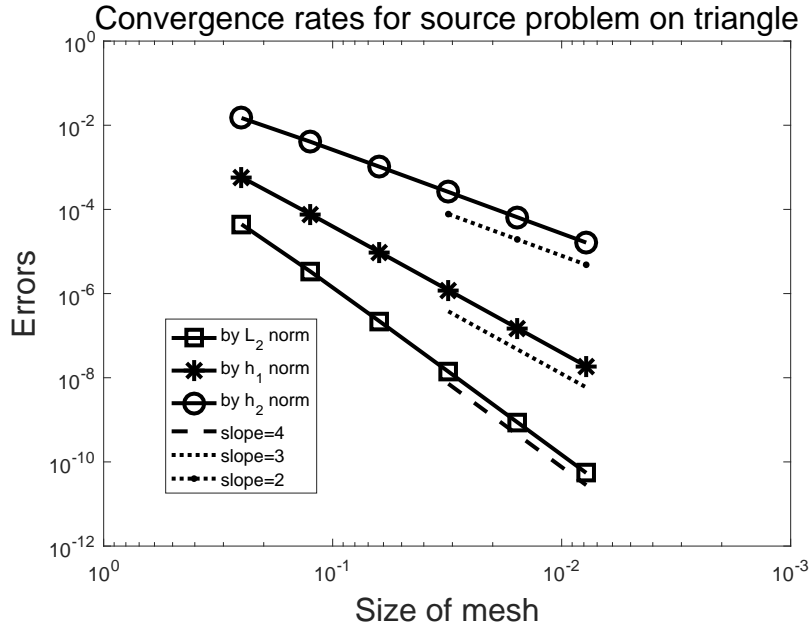
FIGURE 2. The numerical performance by B_{h0}^3 for biharmonic source problem with non-constant coefficient $\delta = 8 + x_1 - x_2$. Y-axis means the numerical error $\|u - u_{h_k}\|$ measured by L_2 or h_1 or h_2 norm. X-axis means the size of mesh.

2.3.2. *For eigenvalue problem.* **Example 4.** Consider the bi-Laplacian eigenvalue problem (7) with constant coefficient $\delta = 1$ on the unit square domain $\Omega_1 = [0, 1]^2$.

Example 5. Consider the bi-Laplacian eigenvalue problem (7) with constant coefficient $\delta = 1$ on the non-convex L-shaped domain $\Omega_3 = [0, 1] \times [0, 1] \backslash [0, \frac{1}{2}) \times (\frac{1}{2}, 1]$.

Here we test on **Example 4** and **Example 5**, respectively. The mesh size of the initial mesh is $h_0 = \frac{1}{2}$. Six levels of uniformly refined triangular meshes are generated for numerical experiments and $h_k = h_{k-1}/2, \ k = 1, 2, 3, 4, 5, 6$. The finest degrees of freedom (short for DOFs) for **Example 4** are 97283. The refinest DOFs for **Example 5** are 146435. We discretize by the second order computational scheme corresponding to B_{h0}^3 space. For each series of meshes, we obtain the computed eigenvalue λ_{h_k}. The convergent orders are computed by

$$log_2 \left(|\frac{\lambda_{k-1} - \lambda_k}{\lambda_{k-2} - \lambda_{k-1}}| \right), \quad k = 3, 4, 5, 6.$$

We present the results of the first six biharmonic eigenvalues showed in Figure 3. For **Example 4**, the results are showed in 3(a). For **Example 5**, the numerical performance is showed in 3(b). We can observe that for convex domain, the convergence rate for eigenvalues approximates 4 which is optimal and consistent with the theoretical expectation. For non-convex domain, the convergence rates are not optimal due to the low regularity of eigenfunctions.

(a)   (b)
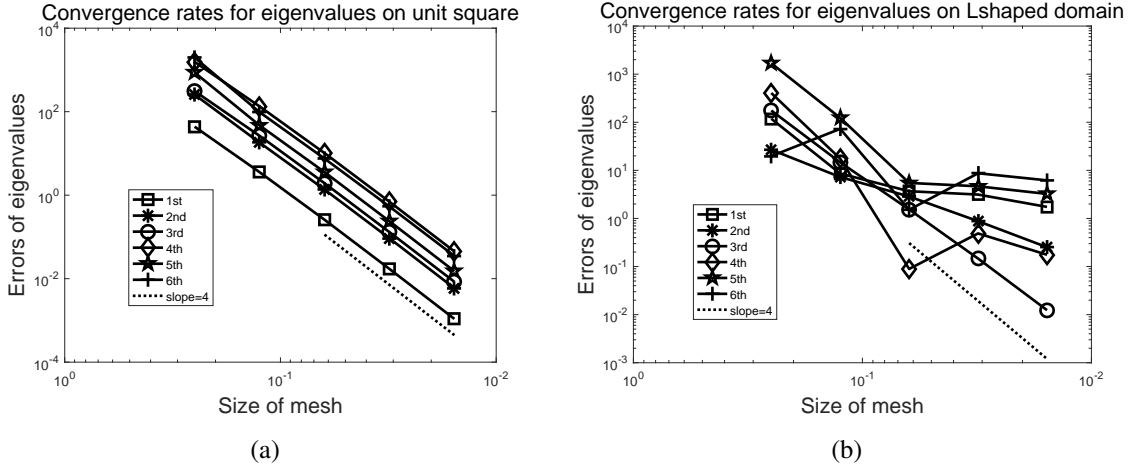
FIGURE 3. The convergence rates for the lowest six real eigenvalues for bi-Laplacian eigenvalue problem by B_{h0}^3. Y-axis means the numerical error $|\lambda - \lambda_{h_k}|$. X-axis means the size of mesh. Left: for **Example 4** which is on square domain; Right: for **Example 5** which is on the non-convex L-shaped domain.

2.3.3. *The B_{h0}^3 scheme for biharmonic eigenvalue problem with non-constant coefficient.* By B_{h0}^3 scheme, the variational formulation for (7) is as followed: find $u \in H_0^2(\Omega)$ and $\lambda \in R$, such

that

$$(\delta\Delta u, \Delta v) = \lambda(u, v), \quad \forall v \in H_0^2(\Omega),$$

The corresponding discretized variational formulation is to find $u_h \in B_{h0}^3$ and $\lambda_h \in R$, such that

$$(\delta\Delta u_h, \Delta v_h) = \lambda_h(u_h, v_h), \quad \forall v_h \in B_{h0}^3.$$

Example 6. Consider the unit square domain $\Omega = [0, 1] \times [0, 1]$ with $\delta(x) = 8 + x_1 - x_2$.

Example 7. Consider the unit square domain $\Omega = [0, 1] \times [0, 1]$ with $\delta(x) = \sqrt{x_1^2 + x_2^2} + 1$.

Here we test on **Example 6** and **Example 7**. The mesh size of the initial mesh is $h_0 = \frac{1}{4}$. Five levels of uniformly refined triangular meshes are generated for numerical experiments and $h_k = h_{k-1}/2$, $k = 1, 2, 3, 4, 5$. The finest degrees of freedom (short for DOFs) are 97283.

For **Example 6**, the lowest ten computed eigenvalues are showed in Table 1. The convergence rate of eigenvalues is 4. The computed eigenvalues tend to give the upper bound.

TABLE 1. The performance of B_{h0}^3 for **Example 6**.

Mesh	1	2	3	4	5	Trend	Ord_λ
λ_1	10374.5195	10345.9954	10343.9256	10343.7882	10343.7794	↘	3.97049
λ_2	43152.3618	43005.8128	42994.7833	42994.0362	42993.9885	↘	3.96937
λ_3	43280.1536	43068.7439	43053.2500	43052.2064	43052.1391	↘	3.95288
λ_4	94720.7844	93650.3052	93568.7622	93563.1966	93562.8374	↘	3.95358
λ_5	138651.7814	138270.0014	138240.9393	138239.0035	138238.8805	↘	3.97531
λ_6	140390.6663	139603.9073	139543.0269	139538.7129	139538.4292	↘	3.92672
λ_7	221070.9885	217636.1630	217378.1490	217360.2947	217359.1410	↘	3.95190
λ_8	221623.7915	218016.9168	217724.6523	217704.3709	217703.0464	↘	3.93657
λ_9	353927.2977	353674.1751	353645.2752	353642.4924	353642.2935	↘	3.80689
λ_{10}	355323.7661	353783.9540	353664.7616	353656.2796	353655.7170	↘	3.91410

For **Example 7**, the lowest ten computed eigenvalues are showed in Table 2. The convergence rate of eigenvalues is 4. The computed eigenvalues tend to give the upper bound.

2.4. **Comparison with Morley element scheme.** We check the Morley element scheme for the eigenvalue problem

(10)
$$\begin{cases} \Delta\delta\Delta u = \lambda u & \text{in } \Omega \\ u = \frac{\partial u}{\partial n} = 0, & \text{on } \partial\Omega. \end{cases}$$

For Morley element, we consider the following variational formulation: find $u \in H_0^2(\Omega)$ and $\lambda \in R$, such that

(11)
$$\alpha(\nabla^2 u, \nabla^2 v) + ((\delta - \alpha)\Delta u, \Delta v) = \lambda(u, v), \quad \forall v \in H_0^2(\Omega),$$

TABLE 2. The performance of B_{h0}^3 for **Example 7**.

Mesh	1	2	3	4	5	Trend	Ord_λ
λ_1	2242.0180	2236.1646	2235.7399	2235.7117	2235.7099	↘	3.97022
λ_2	9154.9841	9110.2819	9107.0020	9106.7807	9106.7664	↘	3.95159
λ_3	9486.4385	9456.1682	9453.8979	9453.7445	9453.7347	↘	3.97046
λ_4	20506.1886	20276.9808	20259.5801	20258.3940	20258.3174	↘	3.95238
λ_5	29816.2535	29732.0314	29725.6516	29725.2265	29725.1994	↘	3.97507
λ_6	30135.9791	29969.1169	29956.0394	29955.1090	29955.0478	↘	3.92537
λ_7	47066.3802	46285.9069	46222.8811	46218.5018	46218.2154	↘	3.93437
λ_8	49000.9675	48277.8380	48224.0164	48220.3162	48220.0777	↘	3.95558
λ_9	75673.2614	75431.9016	75400.3136	75398.0123	75397.8583	↘	3.90143
λ_{10}	75808.5004	75588.8154	75579.7274	75578.9302	75578.8748	↘	3.84894

where $(\nabla^2 u, \nabla^2 v) = \int_\Omega \sum_{s,t=1}^2 \frac{\partial^2 u}{\partial x_s \partial x_t} \frac{\partial^2 v}{\partial x_s \partial x_t} dx$, i.e., the inner product of the Hessian matrices of u and v and α is a constant satisfying $0 < \alpha < \delta_{min}$. The items on the left side of (11) guarantee the coercivity of variational problem.

The Morley element discretization space for $H_0^2(\Omega)$ is denoted by V_h^M. The corresponding discretized variational formulation is: find $u_h \in V_h^M$ and $\lambda_h \in R$, such that

$$(12) \qquad \alpha(\nabla^2 u_h, \nabla^2 v_h) + ((\delta - \alpha)\Delta u_h, \Delta v_h) = \lambda_h(u_h, v_h), \quad \forall v_h \in V_h^M(\Omega).$$

We test the numerical performance of Morley element method on **Example 6** and **Example 7**. For **Example 6**, by Morley element, the lowest ten computed real eigenvalues on three successive grid levels are showed in Figure 4. We can observe that the numerical results are sensitive to the parameter α and greatly depend on the choice of α.

For **Example 7**, the numerical results are showed in Figure 5. For different parameter α, the computed eigenvalues are different. For different $\delta(x)$, the optimal α is also different.

3. A HIGH-ACCURACY SCHEME FOR THE TRANSMISSION EIGENVALUE PROBLEM

For the nonlinear transmission eigenvalue problem (4), the corresponding discretization form is to find $(\tau_h, u_h) \in \mathcal{R} \times B_{h0}^3$ such that $\mathcal{B}(u_h, u_h) = 1$ and

$$(13) \qquad \mathcal{A}_{\tau_h,h}(u_h, v_h) = \tau_h \mathcal{B}_h(u_h, v_h), \quad \forall v_h \in B_{h0}^3.$$

Let $\{\xi_j\}_{j=1}^{N_h}$ be a basis for B_{h0}^3 and the corresponding FEM solution $u_h = \sum_{j=1}^{N_h} u_j \xi_j$, where $\{u_j\}$ corresponds to the standard degrees of freedom for B_{h0}^3 scheme. We need the following matrices in the discrete case and obtain the discretized quadratic eigenvalue problem

$$(14) \qquad (A + \tau B + \tau^2 C)x = 0,$$
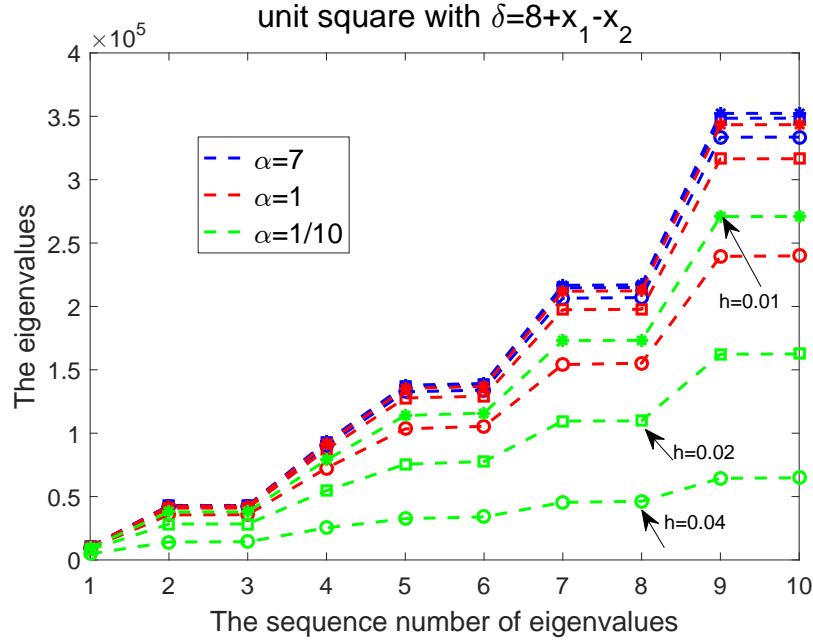
FIGURE 4. The numerical performance by Morley element for biharmonic eigen-value problem with non-constant coefficient $\delta = 8 + x_1 - x_2$. Y-axis means the eigenvalues and X-axis means the sequence number of the lowest ten computed eigenvalues. For a fixed α, the computed real eigenvalues on three successive grid levels are lised corresponding to mesh size $h = 0.04, 0.02, 0.01$.

Matrix	Dimension	Definition
A	$N_h \times N_h$	hessian matrix: $A_{i,j} = \int_\Omega \frac{1}{n-1} \Delta\xi_i \Delta\xi_j dx$
B	$N_h \times N_h$	stiff matrix: $B_{i,j} = \int_\Omega \frac{1}{n-1} \Delta\xi_i \xi_j + \frac{1}{n-1} \xi_i \Delta\xi_j - \nabla\xi_i \cdot \nabla\xi_j dx$
C	$N_h \times N_h$	mass matrix: $C_{i,j} = \int_\Omega \frac{n}{n-1} \xi_i \xi_j dx$

where $x = (u_1, u_2, \cdots, u_{N_h})^T$. The computation of matrices A, B, C involves the numerical integration of basis functions with non-constant coefficients. In practice, we use Gaussian integral formula and calculate the linear combination of function values at gaussian nodes on each triangular element.

For (14), in practical computation, we convert to the linear eigenvalue problem

$$\begin{pmatrix} -B & -A \\ I & O \end{pmatrix} \begin{pmatrix} p_1 \\ p_2 \end{pmatrix} = \tau \begin{pmatrix} C & O \\ O & I \end{pmatrix} \begin{pmatrix} p_1 \\ p_2 \end{pmatrix}$$

and use matlab function "eigs" or "sptarn" to solve. And both p_1 and p_2 are all eigenvectors corresponding to τ.

Theorem 8. *Let (τ, u), (τ_h, u_h) be the solution of (4) and (13), respectively. Under the assumptions of Lemma 3.2 in [18], we can obtain the following results*
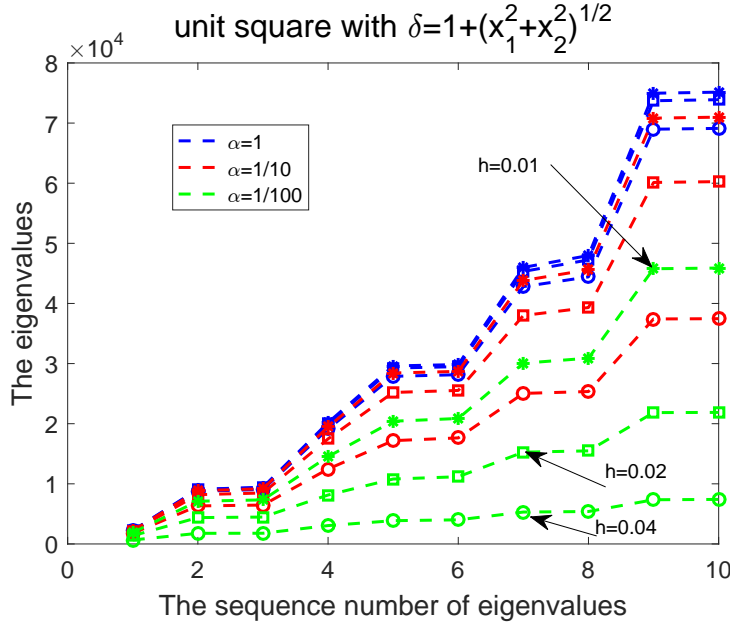
FIGURE 5. The numerical performance by Morley element for biharmonic eigen-value problem with non-constant coefficient $\delta = 1 + \sqrt{x_1^2 + x_2^2}$. Y-axis means the eigenvalues and X-axis means the sequence number of the lowest ten computed eigenvalues. For a fixed α, the computed real eigenvalues on three successive grid levels are lised corresponding to mesh size $h = 0.04, 0.02, 0.01$.

$$\|u - u_h\|_{h_2} \lesssim h^2,$$
$$\|u - u_h\|_1 \lesssim h^4,$$
$$|\tau - \tau_h| \lesssim h^4.$$

3.1. **The numerical performance of the nonconforming B_{h0}^3 scheme.** Here we focus on the case $n(x) > 1$ which is of dominant interest in practice [6]. For the case $0 < n(x) < 1$, it can be treated similarly. Numerical experiments are conducted on a convex domain (a unit square domain $\Omega_1 = [0,1] \times [0,1]$) and a non-convex domain (a L-shaped domain $\Omega_2 = (0,1) \times (0,1)\backslash[\frac{1}{2},1) \times [\frac{1}{2},1)$). Six levels of uniformly refined triangular meshes are generated for numerical experiments. The mesh size of the initial mesh is $h_0 = 0.05$ and $h_k = h_{k-1}/2, k = 1,2,3,4,5,6$. Note that further refinement would lead to very large matrix eigenvalue problems which take too long to solve. All examples are done using Matlab 2016a on a laptop with 16G memory and 2.9GHz Intel Core i7-7500U processor.

For each series of meshes, we obtain the eigenvalue series $\{\lambda_{h_k}\}_{k=1}^6$. The convergent orders are computed by

(15) $$log_2(|\frac{\lambda_{h_l} - \lambda_{h_{l+1}}}{\lambda_{h_{l+1}} - \lambda_{h_{l+2}}}|), \quad l = 1, 2, 3, 4.$$

We consider the following examples.

Example 8. The unit square domain Ω_1 with the constant index of refraction $n(x) = 16$.

The finest degrees of freedom (short for DOFs) are 194566. It costs 251.661752s for the whole calculation. We present the results of the first six real transmission eigenvalues. The eigenvalue approximations ($\lambda_h = \sqrt{\tau_h}$) on the finest mesh are (1.879591, 2.444236, 2.444236, 2.866439, 3.140111, 3.471509).

From Figure 6, we can observe the following phenomena:

(1) The convergence rates of transmission eigenvalues by B_{h0}^3 are 4.

(2) It gives the upper bound for real eigenvalues.

(3) The results by B_{h0}^3 are consistent with those in [13] [14] [16].
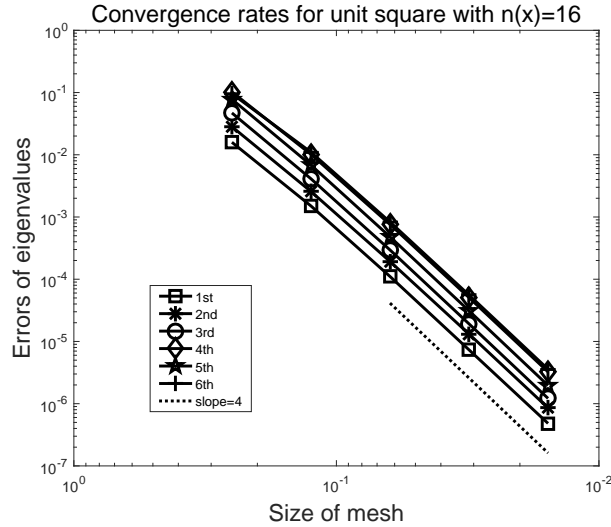
FIGURE 6. The convergence rates for the lowest six real eigenvalues of the unit square with $n(x) = 16$ by B_{h0}^3. Y-axis means $\lambda_{h_k} - \lambda_{h_6}$, as h tends to zero, $\lambda_{h_k} - \lambda_{h_6}$ can be positive or negative; however, as illustrated in the figure, it's positive, here $k = 1, 2, 3, 4, 5$. X-axis means the size of mesh and so are the followings.

Example 9. The unit square domain Ω_1 with the non-constant index of refraction $n(x) = 8 + x_1 - x_2$.

The first six real eigenvalue approximations on the finest mesh are (2.822189, 3.538697, 3.538992, 4.117742, 4.501729, 4.989140) which is consistent with the results in [13] [14] [16]. The convergence rates are showed in Figure 7. It can also be observed that B_{h0}^3 does give the

theoretical predicted fourth convergence rate. And the computed real eigenvalues are monotonically decreasing as the mesh is refined.
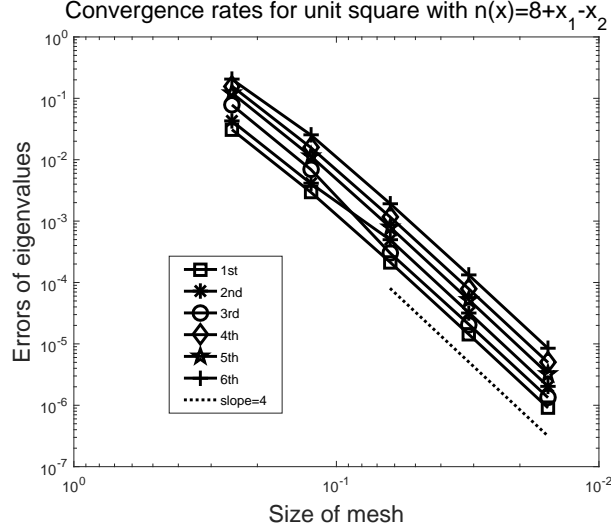
FIGURE 7. The convergence rates for the lowest six real eigenvalues of the unit square with $n(x) = 8 + x_1 - x_2$ by B_{h0}^3. Y-axis means $\lambda_{h_k} - \lambda_{h_6}$, as h tends to zero, $\lambda_{h_k} - \lambda_{h_6}$ can be positive or negative; however, as illustrated in the figure, it's positive, here $k = 1, 2, 3, 4, 5$. X-axis means the size of mesh and so are the followings.

Example 10. The L-shaped domain Ω_2 with the constant index of refraction $n(x) = 24$.

The finest DOFs are 292870. The total calculate time is 467.822844 second. The lowest six real eigenvalues on the finest mesh are (4.275620, 4.555635, 5.172225, 5.271284, 5.984808, 6.081556). Since Ω_2 has a reentrant corner, the eigenfunction has a low regularity. The convergence order for the eigenvalue approximation is less than 4 by the B_{h0}^3 scheme as is showed in Figure 8.

3.2. **Morley element scheme revisited.** In [16] [19], the authors proposed the Morley element to discretize transmission eigenvalue problem. For the non-constant index of refraction $n(x)$, assume $0 < \alpha_s \leq \frac{1}{n(x)-1} \leq \alpha_b$. They transformed the variational formulation to the following form:

$$(16) \qquad \left(\frac{1}{n(x)-1}\Delta u, \Delta v\right) = \left(\left(\frac{1}{n(x)-1} - \alpha\right)\Delta u, \Delta v\right) + (\alpha\nabla^2 u, \nabla^2 v),$$

where $(\nabla^2 u, \nabla^2 v) = \int_\Omega \sum_{s,t=1}^2 \frac{\partial^2 u}{\partial x_s \partial x_t} \frac{\partial^2 v}{\partial x_s \partial x_t} dx$, i.e., the inner product of the Hessian matrices of u and v, α is a constant satisfying $0 < \alpha < \alpha_s$. The form on the right hand of (16) guarantees the
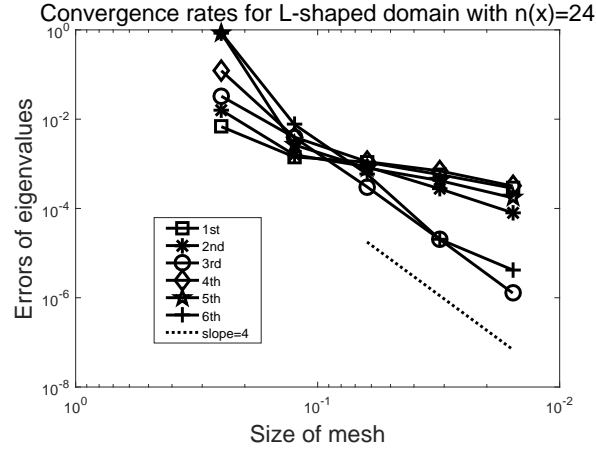
FIGURE 8. The convergence rates for the lowest six real eigenvalues of the L-shaped domain with $n(x) = 24$ by B_{h0}^3. Y-axis means $|\lambda_{h_k} - \lambda_{h_6}|$, as h tends to zero. X-axis means the size of mesh.

coercivity of the variational formulation on $H_0^2(\Omega)$ (c.f. [19]). However, in practical computation, the numerical performance is sensitive to the choice of α. Figure 9 shows the numerical performance by Morley element for unit square domain $\Omega = [0, 1]^2$ with index of refraction $n_1(x) = 8 + x_1 - x_2$. We test on different α. For a fixed α, we record and present the lowest 10 computed real eigenvalues on three successive grid levels. It's observed that the numerical results are greatly dependent on the choice of α. Figure 10 shows the numerical performance for unit square domain with index of refraction $n_2(x) = 18 + x_1^2 + x_2^2$. For different index of refractions, the optimal choice of α is also different.

4. CONCLUDING REMARKS

In this paper, we present a finite element scheme for the Helmholtz transmission eigenvalue problem based on the space B_{h0}^3. Different from most existing nonconforming finite elements, the bilinear form (Δ_h, Δ_h) is coercive on the space B_{h0}^3, and it fits for the problem of operator $\Delta\delta\Delta$, including both the source and eigenvalue problems. Schemes associated with B_{h0}^3 are designed without introducing extra stabilisation mechanism. Numerical experiments illustrate the high accuracy of the schemes. Theoretical analysis will be given soon. The explicit formulation of the local basis functions obtained for easy application will bring in convenience in the future.

REFERENCES

[1] J. An and J. Shen, *A Fourier-spectral-element method for transmission eigenvalue problems*, J. Sci. Comput., **57** (2013), 670–688.
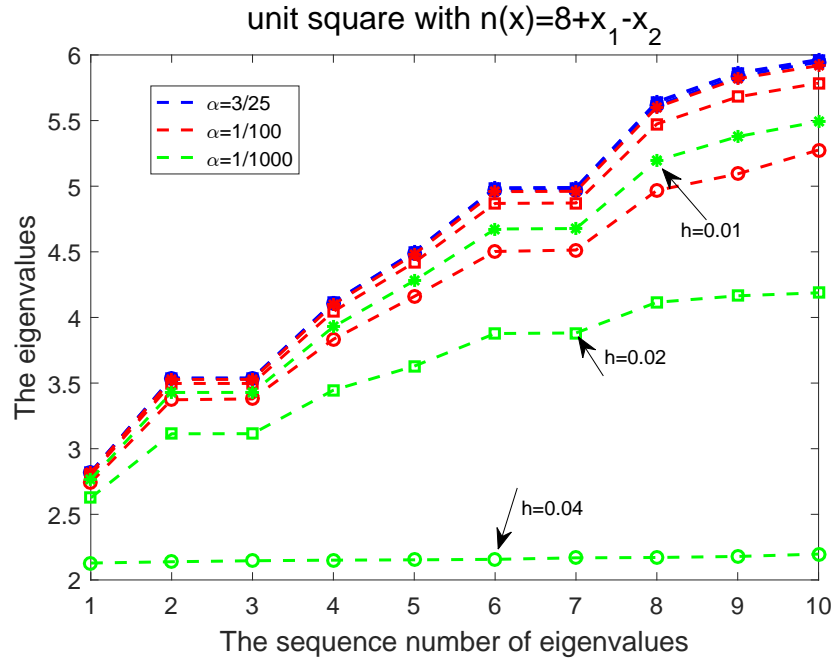
FIGURE 9. The numerical performance by Morley element for transmission eigenvalue problem. Y-axis means the eigenvalues and X-axis means the sequence number of the lowest ten computed real eigenvalues. For a fixed α, the computed real eigenvalues on three successive grid levels are lised corresponding to mesh size $h = 0.04, 0.02, 0.01$.

[2] I. Babuska and J. E. Osborn, *Eigenvalue Problems, in: P. G. Lions and P. G. Ciarlet (eds.) Handbook of Numerical Analysis, Vol. II, Finite Element Methods (Part 1)*, 641–787, NorthHolland, Amsterdam, 1991.

[3] F. Cakoni and H. Haddar, *Transmission eigenvalues in inverse scattering theory*, Inside Out II, G. Uhlmann editor, MSRI Publications, **60** (2012), 526–578.

[4] F. Cakoni and A. Ren, *Transmission eigenvalues and the nondestructive testing of dielectrics*, Inverse Problems, 2008, 24, 065016 (15pp).

[5] J. Camano, R. Rodriguez, P. Venegas, Convergence of a lowest-order finite element method for the transmission eigenvalue problem, Calcolo, **55** (2018).

[6] D. Colton and R. Kress, *Inverse Acoustic and Electromagnetic Scattering Theory, 2nd ed.* Springer-Verlag, New York, 1998.

[7] D. Colton, P. Monk, and J. Sun, *Analytical and computational methods for transmission eigenvalues*, Inver. Probl. **26** (2010), 045011.

[8] H. Geng, X. Ji, J. Sun and L. Xu, *C^0IP method for the transmission eigenvalue problem*, Journal of Scientific Computing, **68** (2016), 326-338.

[9] I. Harris, F. Cakoni and J. Sun, *Transmission eigenvalues and non-destructive testing of anisotropic magnetic materials with voids*, Inverse Problems, 2014, 30: 035016 (21pp).

[10] R. Huang, A. Struthers, J. Sun, and R. Zhang, *Recursive integral method for transmission eigenvalues*, J. Comput. Phys. **327** (2016), 830–840.
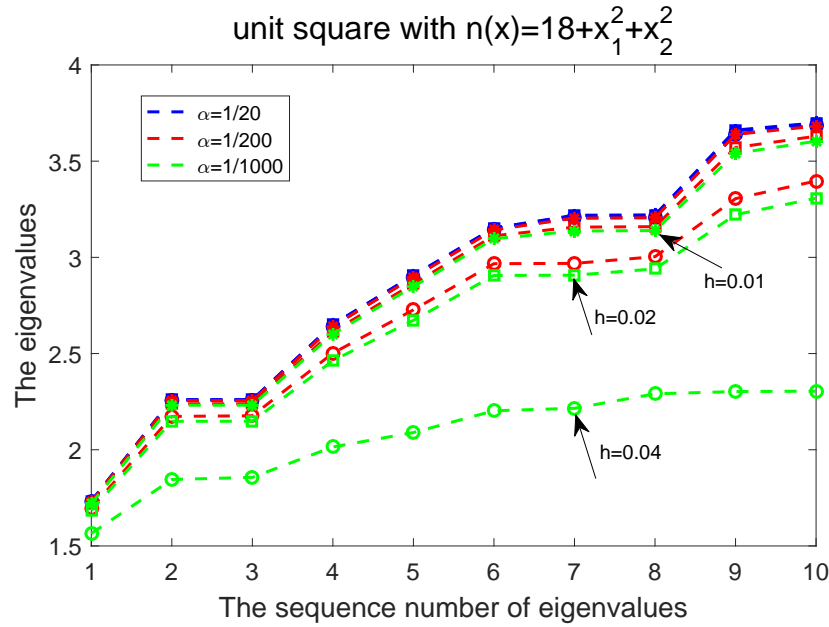
FIGURE 10. The numerical performance by Morley element for transmission eigenvalue problem. Y-axis means the eigenvalues and X-axis means the sequence number of the lowest ten computed real eigenvalues. For a fixed α, the computed real eigenvalues on three successive grid levels are lised corresponding to mesh size $h = 0.04, 0.02, 0.01$.

[11] R. Huang, J. Sun and C. Yang, *Recursive integral method with Cayley transformation*, arXiv:1705.01646, 2017.

[12] X. Ji and H. Liu, *On isotropic cloaking and interior transmission eigenvalue problems*, European Journal of Applied Mathematics, 2018, 29(2): 253-280.

[13] X. Ji, J. Sun, and T. Turner, *A mixed finite element method for Helmholtz transmission eigenvalues*, ACM Trans. Math. Software **8** (2012), Algorithm 922.

[14] X. Ji, J. Sun, and H. Xie, *A multigrid method for Helmholtz transmission eigenvalue problem*, J. Sci. Comput. **60** (2014), 276–294.

[15] A. Kleefeld, *A numerical method to compute interior transmission eigenvalues*. Inver. Probl. **29** (2013), 104012.

[16] X. Ji, Y. Xi and H. Xie, *Nonconforming Finite Element Method for the Transmission Eigenvalue Problem*, Advances in Applied Mathematics and Mechanics, Vol.9, No.1, 2017, 92–103.

[17] T. Li, W. Huang, W. Lin, and J. Liu, *On spectral analysis and a novel algorithm for transmission eigenvalue problems*, J. Sci. Comput. **64** (2015), 83–108.

[18] J. Sun, *Iterative methods for transmission eigenvalues*, SIAM J. Numer. Anal., **49** (2011), 1860–1874.

[19] Y. Xi and X. Ji, *Recursive integral method for the nonlinear non-selfadjoint transmission eigenvalue problem*, Journal of Computational Mathematics. Vol.35, No.6, 2017, 828–838.

[20] Y. Xi, X. Ji, and H. Geng, A C^{0}IP Method of Transmission Eigenvalues for Elastic Waves, Journal of Computational Physics, **374** (2018), 237-248.

[21] Y. Xi, X. Ji, and S. Zhang, A Multi-level Mixed Element Scheme for The Two Dimensional Helmholtz Transmission Eigenvalue Problem, IMA Journal of Numerical Analysis, accepted, 2018.

[22] Y. Yang, H. Bi, H. Li, and J. Han, *Mixed methods for the Helmholtz transmission eigenvalues*, SIAM J. Sci. Comput. **38** (2016), A1383–A1403.

[23] Y. Yang, J. Han and H Bi, *Non-conforming finite element methods for transmission eigenvalue problem*, Computer Methods in Applied Mechanics and Engineering, **307** (2016), 144-163.

[24] S. Zhang, *On optimal finite element schemes for biharmonic equation*, arXiv: 1805.03851.

[25] S. Zhang, *Optimal piecewise cubic finite element schemes for the biharmonic equation on general triangulations*, arXiv: 1903.04897.

School of Science, Nanjing University of Science and Technology, Nanjing 210094, China
E-mail address: xiyingxia@njust.edu.cn

LSEC, Institute of Computational Mathematics and Scientific/Engineering Computing, Academy of Mathematics and System Sciences, Chinese Academy of Sciences, Beijing 100190, People's Republic of China
E-mail address: jixia@lsec.cc.ac.cn

LSEC, Institute of Computational Mathematics and Scientific/Engineering Computing, Academy of Mathematics and System Sciences, Chinese Academy of Sciences, Beijing 100190, People's Republic of China
E-mail address: szhang@lsec.cc.ac.cn